UC Irvine
UC Irvine Previously Published Works

Title

Mapping Molecular Orientation with Phase Sensitive Vibrationally Resonant Sum-Frequency Generation Microscopy

Permalink

https://escholarship.org/uc/item/6vs3z6np

Journal

The Journal of Physical Chemistry B, 117(20)

ISSN

1520-6106

Authors

Han, Yang
Raghunathan, Varun
Feng, Ran-ran
et al.

Publication Date

2013-05-23

DOI

10.1021/jp4022147

**Copyright Information**

Peer reviewed

Mapping Molecular Orientation with Phase Sensitive Vibrationally Resonant Sum-Frequency Generation Microscopy

Yang Han, **Varun Raghunathan**, **Ran-ran Feng**, **Hiroaki Maekawa**, **Chao-Yu Chung**, **Yuan Feng**, **Eric O. Potma**, and **Nien-Hui Ge**[*]
Department of Chemistry, University of California at Irvine, Irvine, California 92697-2025, United States

Abstract

We demonstrate a phase sensitive, vibrationally resonant sum-frequency generation (PSVR-SFG) microscope that combines high resolution, fast image acquisition speed, chemical selectivity, and phase sensitivity. Using the PSVR-SFG microscope, we generate amplitude and phase images of the second-order susceptibility of collagen I fibers in rat tail tendon tissue on resonance with the methylene vibrations of the protein. We find that the phase of the second-order susceptibility shows dependence on the effective polarity of the fibril bundles, revealing fibrous collagen domains of opposite orientations within the tissue. The presence of collagen microdomains in tendon tissue may have implications for the interpretation of the mechanical properties of the tissue.
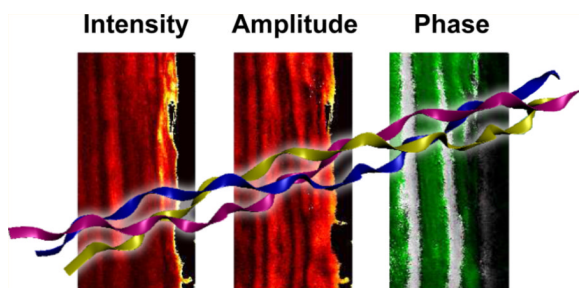
INTRODUCTION

Collagen type I is the main component of tendon tissue, where the collagen molecules associate to form fibrils. On a macroscopic level, the fibrils are organized into fibers, which in turn aggregate and align into parallel or antiparallel arrangements.[1] Although much is known about the molecular structure of the collagen molecule, their arrangement into higher-order three-dimensional structures such as those found in tendon tissue is not very well understood.

Important clues toward collagen organization in tendon tissue have come from optical microscopy studies. Using cross-polarized light microscopy, the aligned fibril arrangements appear as elongated strands with micrometer-scale diameters, which are organized in sheets. Within the plane of the sheet, a periodic modulation of the light intensity is seen in the direction perpendicular to the long axis of fibers, suggesting an undulating arrangement of

[*]**Corresponding Author**nhge@uci.edu. Tel: 949-824-1263..

fibrils.[2] A similar pattern is observed with second harmonic generation (SHG) microscopy, which is sensitive to the noncentrosymmetric arrangement of polarizable units. In the case of collagen, the units correspond to moieties of the molecule that are arranged in a noncentrosymmetric manner, an arrangement that is preserved on a supramolecular scale.[3,4] Polarization sensitive SHG imaging has revealed that the orientation of such moieties is highly conserved along the long axis of the fibril bundle, confirming the long-range order of collagen organization within the tissue.[5–7]

SHG imaging probes the nonresonant, second-order susceptibility $\chi^{(2)}$ of the material. A problem in the interpretation of SHG measurements is that the molecular origin of the nonzero $\chi^{(2)}$ is difficult to determine. Because SHG is performed under nonresonant conditions, the sampled $\chi^{(2)}$ contains off-resonant contributions from several chemical groups. Several attempts have been made to assign the SHG signal to particular groups, most notably the peptide groups of the collagen backbone and the methylene groups of the proline residues.[8–10] However, without selective resonant excitation, assigning the molecular origin of the SHG signal based on symmetry considerations alone remains a challenge.

Another complication of SHG measurements is that the contrast is based on $|\chi^{(2)}|^2$, which is insensitive to the absolute sign of $\chi^{(2)}$. This implies that the technique cannot measure the polarity of the molecular moieties, i.e., it cannot distinguish between the relative orientation of the N-terminus and the C-terminus of the fibrillar units within the sheets. This insensitivity to orientation obscures important structural information about parallel versus antiparallel organization of collagen in tendon tissue.

In order to gain further insight in the macroscopic organization of collagen in tendon tissue, we have developed and applied a new imaging technique based on sum-frequency generation (SFG). Similar to SHG imaging, SFG microscopy probes $\chi^{(2)}$ and is thus sensitive to the same molecular symmetries that are seen in SHG images. However, SFG can be performed under vibrationally resonant conditions, which enables selective excitation of particular chemical groups.[11–14] This is achieved by tuning an infrared (IR) excitation beam into direct resonance with a vibrational mode of the molecule. The electric field of the vibrationally resonant SFG signal (VR-SFG) can be written as

$$E_{\text{SFG},i}=\chi^{(2)}_{ijk}:E_{\text{NIR},j}E_{\text{MIR},k} \quad (1)$$

Here, $\boldsymbol{E}_{\text{SFG}}$, $\boldsymbol{E}_{\text{NIR}}$, and $\boldsymbol{E}_{\text{MIR}}$ are the SFG, near-IR, and mid-IR fields, and the indices (i,j,k) = (x,y,z) indicate their polarization directions. In aligned structures such as collagen, SFG measurements can reveal detailed information about the average orientation of particular molecular groups in the fibril. SFG spectroscopy experiments have indicated that methylene modes in the 2850–3050 cm^{-1} range form a strong achiral contribution to the second-order nonlinearity of collagen.[15] In addition, it has been pointed out that the amide I vibrational mode constitutes a major chiral contribution to the non-vanishing $\chi^{(2)}$ of fibrous collagen type I.[16] Nonetheless, macroscopic SFG measurements provide information that is spatially averaged over typically hundreds of μm^2, thus masking the spatial extent of mode orientation on the micrometer scale. The microscopy implementation of SFG,[17–22] on the other hand, offers an opportunity to examine the orientation of specific chemical groups with submicrometer resolution.

We have recently demonstrated that VR-SFG microscopy with collinear mid-IR and near-IR excitation beams represents a convenient tool for visualizing (bulk) collagen type I in tendon tissue.[23] In this work, we advance SFG microscopy by implementing phase-sensitive detection of the nonlinear signal. It was previously shown in macroscopic SFG

spectroscopic experiments that phase sensitive (PS) detection allows a direct measurement of the amplitude and phase of vibrationally resonant $\chi^{(2)}$ components.[24–27] Here, we extend this principle to microscopic examination of collagen tissue, providing information on the effective polarity of the collagen fibrils within the probing volume. Using PSVR-SFG, we show that the methylene mode exhibits a highly conserved orientation within individual bundles of fibrils. Moreover, we provide evidence that adjacent bundles in tendon tissue exhibit opposite polarities, pointing to a different view of the structural organization of collagen relative to what has previously been deduced from SHG measurements.

MATERIALS AND METHODS

Experimental Setup of PSVR-SFG Microscopy

The experimental setup of the intensity-based VR-SFG microscope has been described elsewhere.[23] Based on the previous setup, we have implemented phase sensitive detection. The idler (3.4 μm mid-IR) and doubled signal (776 nm near-IR) from a 76 MHz picosecond OPO (APE Levante) were combined collinearly and sent into an interferometer as shown in Figure 1. The beams were subsequently split by a 50/50 beam splitter into two arms of the interferometer. In one arm, the beams were focused with a CaF$_2$ lens onto a 5 mm thick type-I LiNbO$_3$ crystal (cut angle $\theta = 41.5°$) to generate the local oscillator (632 nm visible). The collimated local oscillator (LO) was separated from the near-IR and mid-IR beams in this beam path by a bandpass filter. The filtered LO was modulated by an electro-optic phase modulator (PM-Novaphase, EO-PM-R-010). The 10 MHz sync signal from a lock-in amplifier (SR844, Stanford Research) was amplified to 10 V$_{peak-to-peak}$ to drive the phase modulator. The phase modulated LO was recombined with the beams from the other arm by a dichroic mirror that transmits near-IR and mid-IR beams but reflects the LO. The output of the interferometer includes three different colors, near-IR (100 mW), mid-IR (30 mW), and LO (power tunable with neutral density filters). All three beams were steered into a commercial microscope (Olympus IX71) with the same polarization state. A reflective objective (0.65 NA) was used to focus the beams onto the sample. The SFG signal and LO were collected by a photomultiplier tube in the forward direction through a bandpass filter (630 nm ± 20 nm). The current signal was fed to the lock-in amplifier for demodulation of the 10 MHz signal.

Preparation of Collagen Samples

Collagen samples were extracted from rat tail tendon tissue and flattened between two glass slides to slices of ~100 μm thickness. For PSVR-SFG measurements, the collagen segment was cut into two halves and placed on the front surface of a piece of z-cut quartz, facing toward the incident laser beams. One segment was rotated in plane by 180°, aligned in an antiparallel orientation with respect to the other segment, with a small space between them. Unless otherwise noted, the longitudinal axes of fiber strands were aligned with the polarization of the mid-IR excitation beam.

Determining Phase by PSVR-SFG Microscopy

The SFG signal is described by eq 1. The nonlinear susceptibility of the sample, $\chi^{(2)}$, is a complex quantity. The phase of the resulting VR-SFG field is determined by the phase of $\chi^{(2)}$. The phase sensitive signal can be written as

$$I_{PS} \propto E_{MIR} E_{NIR} E_{LO} \left(\mathrm{Re} \quad \chi^{(2)} + \mathrm{i} \quad \mathrm{Im} \quad \chi^{(2)} \right) \mathrm{e}^{\mathrm{i}\Delta\varphi} + c.c.$$

Here, E_{MIR}, E_{NIR}, and E_{LO} represent the amplitude of the mid-IR, near-IR, and LO, respectively. $\Delta\varphi$ stands for the phase shift of the LO field with respect to the product fields $E_{MIR}E_{NIR}$. In our experiment, the phase of the LO was changed with the angular modulation frequency ω_M:

$$\Delta\varphi = \varphi_{MIR} + \varphi_{NIR} - \varphi LO = \Delta\varphi_0 + A \sin \omega_M t$$

where A is the amplitude of the modulation and $\Delta\varphi_0$ is the unmodulated part of $\Delta\varphi$. Upon substituting $\Delta\varphi$ into $e^{i\Delta\varphi}$, we find

$$e^{i\Delta\varphi} = e^{i\Delta\varphi_0} \left[\cos\left(A \sin \omega_M t\right) + i \sin\left(A \sin \omega_M t\right) \right]$$

The cosine and sine terms can be expanded into the following Fourier series:

$$\cos\left(A \sin \omega_M t\right) = J_0(A) + 2\sum_{n=1}^{\infty} J_{2n}(A) \cos 2n\omega_M t$$

$$\sin\left(A \sin \omega_M t\right) = 2\sum_{n=1}^{\infty} J_{2n-1}(A) \sin(2n-1)\omega_M t$$

$J_m(A)$ is the Bessel function of order m evaluated at A. Only one term carries the fundamental modulation frequency in these expansions. The other terms are not detected by the lock-in amplifier. Effectively,

$$e^{i\Delta\varphi} \approx 2ie^{i\Delta\varphi_0} J_1(A) \sin \omega_M t$$

We next consider two settings of the interferometer. First, we set $\Delta\varphi_0 = -\pi/2$; we then find

$$I_{PS} \propto 4J_1(A) E_{MIR} E_{NIR} E_{LO} \text{Re} \chi^{(2)} \sin \omega_M t$$

Note that for this setting the amplitude of the phase sensitive signal is governed by the real part of the material response. Consequently, the demodulated signal is directly proportional to Re $\chi^{(2)}$. Second, we set $\Delta\varphi_0 = -\pi$, which gives rise to the following measured intensity:

$$I_{PS} \propto 4J_1(A) E_{MIR} E_{NIR} E_{LO} \text{Im} \chi^{(2)} \sin \omega_M t$$

For this setting, the demodulated signal is proportional to Im $\chi^{(2)}$. In the determination of the phase, a piece of z-cut quartz was used as a reference. We can adjust $\Delta\varphi_0$ with the piezo stage (PS1 in Figure 1), to maximize the quartz signal. Given that the quartz signal arises from $\chi^{(2)}$ components that are purely real, when it is maximized, we have $\Delta\varphi_0 = -\frac{\pi}{2}$. With this experimental setting, the real part of the second order response can be obtained as I_{real}. Similarly, when the quartz signal is set to zero, the contribution from the imaginary part can be collected as I_{imag}. The phase of $\chi^{(2)}_{collagen}$ can be determined from the in-phase and quadrature-phase components as

$$\varphi_{\text{collagen}} = \begin{cases} \tan^{-1} \frac{I_{\text{imag}}}{I_{\text{real}}} & \text{if} \quad I_{\text{real}} > 0 \\ \tan^{-1} \frac{I_{\text{imag}}}{I_{\text{real}}} + \pi & \text{if} \quad I_{\text{real}} < 0 \quad \text{and} \quad I_{\text{imag}} \geq 0 \\ \tan^{-1} \frac{I_{\text{imag}}}{I_{\text{real}}} - \pi & \text{if} \quad I_{\text{real}} < 0 \quad \text{and} \quad I_{\text{imag}} \leq 0 \\ \frac{\pi}{2} & \text{if} \quad I_{\text{real}} = 0 \quad \text{and} \quad I_{\text{imag}} > 0 \\ -\frac{\pi}{2} & \text{if} \quad I_{\text{real}} = 0 \quad \text{and} \quad I_{\text{imag}} < 0 \end{cases}$$

Using this definition, we can resolve the phase of possible $\chi_{\text{collagen}}^{(2)}$ within the interval $[-\pi, \pi]$ as pictorially shown in Figure 2: The first case corresponds to points A and D in the complex plane, the second case corresponds to point B, and the third case corresponds to point C.

VR-SFG Spectroscopic Measurements

For the VR-SFG spectroscopy measurements, we used a regenerative amplifier (Spitfire Ace, Newport-Spectra Physics) which generated 90 fs pulses with a center wavelength of 800 nm at a 2-kHz repetition rate. A portion of the 800 nm beam was directed through a home-made spectral shaper and was spectrally narrowed to 1.4 nm fwhm. Another portion of the 800 nm beam was used to pump an optical parametric amplifier (OPA) to generate broadband mid-IR pulses of 220 cm^{-1} fwhm at around 3.4 μm. The shaped picosecond 800 nm beam and the mid-IR beam were arranged in a copropagating geometry with incident angles of 45° and 67°, respectively, and the reflected SFG signal was detected by a spectrograph (SP-2358, Princeton Instrument) combined with a CCD camera (DU920P-BR-DD, Andor Technology). The polarizations of the incident beams and signal were individually controlled by half-wave plates and polarizers in the measurements with different polarizations.

Molecular Dynamics Simulation of a Model [(PPG)$_{10}$]$_3$ Triple Helix

The initial [(PPG)$_{10}$]$_3$ triple helix structure was obtained from the protein data bank (PDB ID: 1K6F chains A, B, and C).[28] The protein was dissolved in 4103 TIP3 water[29] to form a 34 Å × 34 Å × 113 Å box. The following minimization and simulation were carried out with the NAMD 2.6 package.[30] We used CHARMM22 force fields with CMAP correction.[31,32] Periodic boundary conditions were applied in three dimensions, and electrostatic interactions were calculated using the PME method.[33] Temperature was controlled by the Nosé–Hoover–Langevin piston method.[14,34] Bond lengths involving hydrogen/deuterium atoms were constrained using the SHAKE algorithm.[35] The integration time step was set to 1 fs. To maintain the crystal structure unaltered during the minimization and pre-equilibration step, the following measures were taken. The water box was allowed to equilibrate for 10,000 steps with the protein coordinates fixed. Then the protein backbone and carbonyl oxygen atoms were restrained with an additional force, while the rest of the system was allowed to move to minimize the potential energy. The initial temperature of the system was set to 0 K. After minimization, the system was immersed into a Langevin bath to reach 285 K. The system was equilibrated in the NVT ensemble with the backbone atoms restrained for 600 ps, and then allowed to equilibrate in the NPT ensemble while slowly reducing the restraint to zero in 1.4 ns. After that, the system was allowed to freely propagate for 56 ns. The last 100 ps trajectory was collected for the analysis of the orientation of the methylene groups.

RESULTS AND DISCUSSION

SFG Spectroscopic Study of Collagen

To investigate the spectral characteristics of the SFG signal from collagen samples in the CH stretching range, we performed spectroscopic studies using a home-built VR-SFG spectrometer. Two peaks are observed in the CH stretching region: one centered at 2966 cm^{-1} and the other 2890 cm^{-1}. The 2966 cm^{-1} peak is much weaker in the ppp polarization than in the ssp polarization. We attribute the origin of the 2966 cm^{-1} peak to the Fermi resonance between the CH_2 symmetric stretch and the overtone of CH_2 symmetric bending mode based on two reasons. First, the Fermi resonance band has the same symmetry as the CH_2 symmetric stretching mode and thus will exhibit similar polarization dependence.[36] Second, this assignment is consistent with a previous VR-SFG study of collagen[15] and another study of air/diol interfaces that also assigned the band at 2954 cm^{-1} to Fermi resonance.[36]

Polarization Dependent Imaging of Collagen with VR-SFG Microscopy

Figure 4 shows the result of a polarization dependent study of a segment of rat tail tendon tissue on a glass slide, conducted in the intensity detection mode. Strong signals and high contrast are observed when the long axes of collagen fibers are placed parallel to the polarization of the mid-IR beam. The result indicates that the spatially averaged orientation of the vibrational transition dipole of the SFG-active methylene units is along the long fiber axis. However, the absolute orientation of the transition dipole remains ambiguous. Although this information is contained in the second-order susceptibility $\chi^{(2)}$, it is inaccessible when the signal is detected as the square modulus of the field. As shown below, phase sensitive detection preserves the phase information, retrieving details on molecular orientation.

Collagen Imaging with PSVR-SFG Microscopy

A periodically poled $LiNbO_3$ crystal was used to test the capability of the PSVR-SFG microscope. We clearly observed the phase shift between different domains with opposite crystal orientation (data not shown). Then we used PSVR-SFG microscopy to visualize a tendon segment placed on top of a piece of *z*-cut quartz. The results are shown in Figure 5. The elongated fiber structure is observed with great detail in both the intensity and amplitude images in Figure 5a and Figure 5b. Individual strands within the tendon tissue can be clearly recognized. Moreover, the phase sensitive measurement exhibits two interesting patterns (Figure 5c). First, the phase within a longitudinal fibrous domain in the tendon tissue appears largely continuous on a length scale larger than 50 μm. This implies that, on this length scale, the effective orientation of the SFG active methylene groups within the fibers is maintained. Second, within the sheet of fibers, there are subdomains which present a ~180° phase difference between aligned strands, such as between the gray and green strands in Figure 5c. Figure 5e and Figure 5f present a slice across the amplitude and phase images. Sharp changes in the phase are observed across ~10 μm domains, which appear as demarcated fibers. At the points of phase change, the amplitude reaches minima, indicating destructive interference between 180° phase-shifted signals.

The origin of the ~180° phase difference is quite interesting. As suggested by previous SFG studies, a 180° phase shift can be explained by a sign reversal of $\chi^{(2)}$, introduced because of an orientational reversal of the SFG active units.[37–39] In our measurement, when we took two consecutive tendon segments and manually reversed one of them, thus placing them in an antiparallel fashion, we observed the expected 180° phase difference between the segments.

A closer look at the distribution of the phase from all pixels is shown in Figure 5d. Three distinct peaks are observed. The peak centered at 0° is mainly originated from the nonresonant signal of z-cut quartz. The other two peaks centered at 63° and –135° are mainly the response from collagen. They are separated by 198°, which is fairly close to the 180° phase shift we expected. We have made measurements on different samples, and the resulting phase shift is always close to 180°, suggesting that this observation is not an anomaly.

In the ideal case that the mid-IR beam is exactly on resonance with all vibrators in the sample, the real part of collagen $\chi^{(2)}$ is zero and Figure 5d is expected to show two delta functions at ±90°, corresponding to oppositely oriented fibers. However, several factors could affect the actual value of the measured phase. One reason is that the laser was not exactly on resonance. The difference of a few wavenumbers could cause considerable phase shifts away from the precisely on-resonant condition. In our experiment, the mid-IR excitation beam was centered at 2950 cm^{-1}, which is 16 cm^{-1} from the resonance at 2966 cm^{-1}. The phase shift can be estimated from the SFG spectrum measured in Figure 3a. We assume that the ssp spectrum is proportional to (Im $\chi^{(2)}$)^2. The real part can be calculated from it using the Kramers–Kronig relation.[40] This assumption is valid when the laser is near resonance with the vibrational mode and the nonresonant contributions can be ignored. As shown in the calculated phase in Figure 3b, when the mid-IR beam is tuned to 2950 cm^{-1} as in the PSVR-SFG microscopic measurement, the phase of $\chi^{(2)}$ is 73° whereas that of $-\chi^{(2)}$ is –107°, which follows the same trend as the experimentally measured phase distribution (Figure 5d). The second reason is the presence of spectral inhomogeneity and hence not all vibrators can be exactly on resonance. This would explain the width of the peaks in the phase distribution. Another possible reason is that the response from the quartz beneath the collagen fiber contributes to the in-phase signal, affecting the measurement of the real part of the response of the collagen fibers. The quartz contribution to the real part will reduce the phase difference between the two collagen peaks. The difference between the two peaks is relatively close to 180°, and hence the contribution from quartz can be neglected.

Theoretical Model of the Phase Change

We can explain the ~180° phase difference in the case of collagen by a simple model. As shown in Figure 6, the longitudinal axis of a collagen superhelix is fixed along the z-axis and the laser beams propagate along the x-axis in the laboratory frame coordinates. The molecular frame coordinates of a single methylene group are defined with the a-axis located on the CH$_2$ plane and the c-axis bisecting the HCH angle, parallel to the transition dipole moment of the symmetric CH stretching vibration. The transformation from the molecular frame to the lab frame can be achieved through rotation around the Euler angles (θ, φ, and ψ).

Our analysis of a molecular dynamics simulation of a model collagen peptide, [(PPG)$_{10}$]$_3$, shows that the distribution of methylene groups within a single triple helix is not isotropic. The angle distributions of residue-specific CH$_2$ groups are shown in Figure 7. It is clear from the figure that the CH$_2$ groups in one triple helix are narrowly distributed at certain θ angles, and the a angle distribution is clustered but covers the whole range. Many such triple helices reside in a segment of rat tail tendon tissue. The longitudinal axes of the helices are aligned, but the rotation along the longitudinal axis can be random. Therefore, it is reasonable to assume that the CH$_2$ groups from a large number of helices within our excitation volume have an even distribution along the angle a, i.e., the orientation distribution is rotationally isotropic with respect to the longitudinal axis.

For rotationally isotropic systems, there are 7 nonzero achiral terms in the second order susceptibility, namely, $\chi_{zzz}^{(2)}$, $\chi_{xxz}^{(2)}=\chi_{yyz}^{(2)}$, $\chi_{xzx}^{(2)}=\chi_{yzy}^{(2)}$, and $\chi_{zxx}^{(2)}=\chi_{zyy}^{(2)}$, in the laboratory frame defined in Figure 6.[36] They are related to the hyper-polarizability of the methylene group through the same transformation that connects the laboratory frame and the molecular frame. Due to the rotational isotropy, the relation is simplified by integration over the two Euler angles (φ and ψ):[41,42]

$$
\begin{aligned}
\chi_{zzz}^{(2),\text{ss}} =\ & \tfrac{1}{2}N_\text{s}\left(\beta_{aac}+\beta_{bbc}\right)\langle\cos\theta\rangle - \tfrac{1}{2}N_\text{s}\left(\beta_{aac}+\beta_{bbc}-2\beta_{ccc}\right)\langle\cos^3\theta\rangle \\
\chi_{xxz}^{(2),\text{ss}} =\ & \chi_{yyz}^{(2),\text{ss}}=\tfrac{1}{4}N_\text{s}\left(\beta_{aac}+\beta_{bbc}+2\beta_{ccc}\right)\langle\cos\theta\rangle+\tfrac{1}{4}N_\text{s}\left(\beta_{aac}+\beta_{bbc}-2\beta_{ccc}\right)\langle\cos^3\theta\rangle \\
\chi_{zxx}^{(2),\text{ss}} =\ & \chi_{xzx}^{(2),\text{ss}}=\chi_{zyy}^{(2),\text{ss}}=\chi_{yzy}^{(2),\text{ss}}= -\tfrac{1}{4}N_\text{s}\left(\beta_{aac}+\beta_{bbc}-2\beta_{ccc}\right)\left(\langle\cos\theta\rangle-\langle\cos^3\theta\rangle\right)
\end{aligned}
$$

Here, $\beta_{ijk}(i,j,k=a,b,c)$ stands for the molecular hyper-polarizability, and N_s is the density of molecules within the focal volume. In the PSVR-SFG microscopic measurements, the near-IR, mid-IR, and local oscillator were all polarized along the longitudinal axis of collagen fibers. Although a reflective objective was used for tight focusing, the electric field at the focus is predominantly z-polarized based on a simulation. Hence the $\chi_{zzz}^{(2)}$ term dominates the SFG signal. When one collagen segment is rotated with respect to the x-axis by 180°, θ is changed into $\pi-\theta$. The second order response is then

$$
\chi_{zzz}^{(2)}\left(\pi-\theta\right)=-\chi_{zzz}^{(2)}\left(\theta\right)
$$

As we observed experimentally, the theoretical estimation also shows that reversing collagen orientation causes a phase change of 180°. We thus interpret the observed phase difference as the presence of an effective polarity of the fiber segments.

DISCUSSION

In this work, we have used PSVR-SFG imaging for examining the organization of (bulk) collagen in rat tail tendon tissue. The use of PSVR-SFG enabled us to investigate two new aspects of collagen that have previously been difficult to assess with SHG microscopy. First, the vibrationally resonant properties of SFG have allowed us to select a particular mode that contributes to the second-order nonlinearity of collagen type I. The selected mode at 2966 cm^{-1}, which has previously been attributed to the vibrations of the methylene group, makes it possible to directly relate the nonlinear signal to specific chemical groups of the aligned collagen fibrils. Using polarization dependent SFG imaging, we have found that the effective orientation of the SFG-active methylene mode shows a maximum in the direction of the fiber axis. This observation is in agreement with previous macroscopic SFG[15] and microscopic SHG studies.[8]

Second, the phase sensitive detection reveals well-demarcated phase changes in the SFG response. A possible origin of such phase changes is the variation of dispersive properties in the tendon tissue, which could produce a spatially dependent chromatic phase shift between the excitation beams and the local oscillator. Height and density variations may contribute to the latter effect. Nonetheless, such variations are expected to generate phase variations over a more extended angular range, rather than the narrow range of phase shifts observed in Figure 5d. The measured phase distribution falls into two narrow ranges separated by ~180°. Using the quartz phase as a reference, we have been able to carefully examine the sign of the nonlinear signal in the collagen material. The presence of distinct well-defined phase domains strongly suggests that the PSVR-SFG map reflects a sign reversal in the Im $\chi^{(2)}$ of fibrillar segments in the tissue. Importantly, the phase remains virtually constant within a

fibril bundle, but may change between adjacent bundles. In our interpretation, flipping of the phase corresponds to a reversal of the collagen fibril orientation, i.e., the fibril is rotated such that the N-terminus and C-terminus switch positions in the frame of the tissue. This interpretation supports a model that includes the existence of fibrillar domains where, on average, the collagen fibrils exhibit a preferred orientation.

We note that a reversal of the sign of $\chi^{(2)}$ may, in principle, also be observed in phase sensitive SHG. Recent tomographic work has demonstrated that interferometric detection of SHG signals gives access to phase information that cannot be probed with conventional SHG imaging.[27,29,43] Indeed, our observation is in concert with recent phase sensitive SHG measurements on collagen (through private communication with François Légaré, Institut National de la Recherche Scientifique, Centre Énergie Matériaux et Télécommunications, Canada). Nonetheless, phase-sensitive SFG enables a direct identification of the molecular modes whose differences in orientation are responsible for the sign reversal, providing a more complete molecular picture than what can be obtained with SHG.

It is known that fibrils can exhibit a definite polarity on the nanoscopic scale. Previous studies using piezoresponse force microscopy observed nanodomains with opposite polar axis orientation.[44,45] It was deduced that each nanodomain consists of 2–3 fibrils on average. Other studies have shown that sustained polarity of collagen fibrils may prevail up to a ~10 μm length scale along the strand.[45,46] Our PSVR-SFG studies provide evidence that the average polarity can extend beyond a ~50 μm length scale along a fibrous strand. The existence of microdomains with alternating effective polarity of collagen molecules has not been observed before on this length scale. It should be noted that the resolution of this far-field imaging technology is insufficient to determine absolute levels of orientational inhomogeneity within the probing volume. Instead, our measurements report the existence of domains where the average orientation of collagen molecules is in a preferred direction.

CONCLUSION

In conclusion, we have demonstrated VR-SFG microscopy with phase sensitive detection and applied it to investigate collagen orientation in rat tail tendon tissue. The microscope inherited the advantages from its intensity-based predecessor, such as the fast imaging capabilities and a high lateral resolution (0.6 μm). Using phase sensitive detection of the SFG signal, we have demonstrated that the real and imaginary part of the nonlinear susceptibility can be acquired separately, enabling generation of images with contrast based on the amplitude and phase of $\chi^{(2)}$. The phase image suggests the existence of domains with a 180° phase difference resulting from the orientation reversal of collagen fibers. The existence of fibrous domains that exhibit a distinct polarity of collagen molecules relative to adjacent domains may have implications for the interpretation of the mechanical properties of tendon tissue.

Acknowledgments

REFERENCES

1. Hulmes DJS. Building Collagen Molecules, Fibrils, and Suprafibrillar Structures. J. Struct. Biol. 2002; 137:2–10. [PubMed: 12064927]

2. Giraud-Guille M-M, Belamie E, Mosser G, Helary C, Gobeaux F, Vigier S. Liquid Crystalline Properties of Type I Collagen: Perspectives in Tissue Morphogenesis. C. R. Chimie. 2008; 11:245–252.

3. Cox G, Kable E, Jones A, Fraser I, Manconi F, Gorrell MD. 3-Dimensional Imaging of Collagen Using Second Harmonic Generation. J. Struct. Biol. 2003; 141:53–62. [PubMed: 12576020]

4. Yeh AT, Nassif N, Zoumi A, Tromberg BJ. Selective Corneal Imaging Using Combined Second-Harmonic Generation and Two-Photon Excited Fluorescence. Opt. Lett. 2002; 27:2082–2084. [PubMed: 18033448]

5. Plotnikov SV, Millard AC, Campagnola PJ, Mohler WA. Characterization of the Myosin-Based Source for Second-Harmonic Generation from Muscle Sarcomeres. Biophys. J. 2006; 90:693–703. [PubMed: 16258040]

6. Psilodimitrakopoulos S, Santos SICO, Amat-Roldan I, Thayil AKN, Artigas D, Loza-Alvarez P. In Vivo, Pixel-Resolution Mapping of Thick Filaments' Orientation in Nonfibrilar Muscle Using Polarization-Sensitive Second Harmonic Generation Microscopy. J. Biomed. Opt. 2009; 14:014001. [PubMed: 19256689]

7. Tiaho F, Recher G, RouEde D. Estimation of Helical Angles of Myosin and Collagen by Second Harmonic Generation Imaging Microscopy. Opt. Express. 2007; 15:12286–12295. [PubMed: 19547597]

8. Su P-J, Chen W-L, Chen Y-F, Dong C-Y. Determination of Collagen Nanostructure from Second-Order Susceptibility Tensor Analysis. Biophys. J. 2011; 100:2053–2062. [PubMed: 21504742]

9. Mitchell SA, McAloney RA, Moffatt D, Mora-Diez N, Zgierski MZ. Second-Harmonic Generation Optical Activity of a Polypeptide Alpha-Helix at the Air/Water Interface. J. Chem. Phys. 2005; 122:114707–114708. [PubMed: 15836243]

10. Deniset-Besseau A, Duboisset J, Benichou E, Hache F, Brevet P-F, Schanne-Klein M-C. Measurement of the Second-Order Hyperpolarizability of the Collagen Triple Helix and Determination of Its Physical Origin. J. Phys. Chem. B. 2009; 113:13437–13445. [PubMed: 19754079]

11. Shen YR. Surface Properties Probed by Second-Harmonic and Sum-Frequency Generation. Nature. 1989; 337:519–525.

12. Eisenthal KB. Equilibrium and Dynamic Processes at Interfaces by Second Harmonic and Sum Frequency Generation. Annu. Rev. Phys. Chem. 1992; 43:627–661.

13. Howell C, Diesner M-O, Grunze M, Koelsch P. Probing the Extracellular Matrix with Sum-Frequency-Generation Spectroscopy. Langmuir. 2008; 24:13819–13821. [PubMed: 19053661]

14. Diesner M-O, Welle A, Kazanci M, Kaiser P, Spatz J, Koelsch P. In Vitro Observation of Dynamic Ordering Processes in the Extracellular Matrix of Living, Adherent Cells. Biointerphases. 2011; 6:171–179. [PubMed: 22239810]

15. Rocha-Mendoza I, Yankelevich DR, Wang M, Reiser KM, Frank CW, Knoesen A. Sum Frequency Vibrational Spectroscopy: The Molecular Origins of the Optical Second-Order Nonlinearity of Collagen. Biophys. J. 2007; 93:4433–4444. [PubMed: 17766339]

16. Reiser KM, McCourt AB, Yankelevich DR, Knoesen A. Structural Origins of Chiral Second-Order Optical Nonlinearity in Collagen: Amide I Band. Biophys. J. 2012; 103:2177–2186. [PubMed: 23200051]

17. Florsheimer M, Brillert C, Fuchs H. Chemical Imaging of Interfaces by Sum Frequency Microscopy. Langmuir. 1999; 15:5437–5439.

18. Hoffmann DMP, Kuhnke K, Kern K. Sum-Frequency Generation Microscope for Opaque and Reflecting Samples. Rev. Sci. Instrum. 2002; 73:3221–3226.

19. Hernandez M, Chinwangso P, Cimatu K, Srisombat L, Lee TR, Baldelli S. Chemial Imaging and Distribution Analysis of Mono-, Bi-, and Tridentate Alkanethiol Self-Assembled Monolayers on Gold by Sum Frequency Generation Imaging Microscopy. J. Phys. Chem. C. 2011; 115:4688–4695.

20. Inoue K, Fujii M, Sakai M. Development of a Non-Scanning Vibrational Sum-Frequency Generation Detected Infrared Super-Resolution Microscope and Its Application to Biological Cells. Appl. Spectrosc. 2010; 64:275–281. [PubMed: 20223061]

21. Miyauchi Y, Sano H, Okada J, Yamashita H, Mizutani G. Simultaneous Optical Second Harmonic and Sum Frequency Intensity Image Observation of Hydrogen Deficiency on a H-Si(111) 1×1 Surface After IR Light Pulse Irradiation. Surf. Sci. 2009; 603:2972–2977.

22. Nakai IF, Tachioka M, Ugawa A, Ueda T, Watanabe K, Matsumoto Y. Molecular Structure and Carrier Distributions at Semiconductor/Dielectric Interfaces in Organic Field-Effect Transistors Studied with Sum Frequency Generation Microscopy. Appl. Phys. Lett. 2009; 95:243304.

23. Raghunathan V, Han Y, Korth O, Ge N-H, Potma EO. Rapid Vibrational Imaging With Sum Frequency Generation Microscopy. Opt. Lett. 2011; 36:3891–3893. [PubMed: 21964132]

24. Shen YR, Ostroverkhov V. Sum-Frequency Vibrational Spectroscopy on Water Interfaces: Polar Orientation of Water Molecules at Interfaces. Chem. Rev. 2006; 106:1140–1154. [PubMed: 16608175]

25. Stiopkin IV, Jayathilake HD, Bordenyuk AN, Benderskii AV. Heterodyne-Detected Vibrational Sum Frequency Generation Spectroscopy. J. Am. Chem. Soc. 2008; 130:2271–2275. [PubMed: 18217755]

26. Yamaguchi S, Tahara T. Heterodyne-Detected Electronic Sum Frequency Generation: "Up" Versus "down" Alignment of Interfacial Molecules. J. Chem. Phys. 2008; 129:101102. [PubMed: 19044899]

27. Hua W, Chen X, Allen HC. Phase-Sensitive Sum Frequency Revealing Accommodation of Bicarbonate Ions, and Charge Separation of Sodium and Carbonate Ions within the Air/Water Interface. J. Phys. Chem. A. 2011; 115:6233–6238. [PubMed: 21513316]

28. Berisio R, Vitagliano L, Mazzarella L, Zagari A. Crystal Structure of the Collagen Triple Helix Model [(Pro-Pro-Gly)$_{10}$]$_3$. Protein Sci. 2002; 11:262–270. [PubMed: 11790836]

29. Jorgensen WL, Chandrasekhar J, Madura JD, Impey RW, Klein ML. Comparison of Simple Potential Functions for Simulating Liquid Water. J. Chem. Phys. 1983; 79:926–935.

30. Phillips JC, Braun R, Wang W, Gumbart J, Tajkhorshid E, Villa E, Chipot C, Skeel RD, Kale L, Schulten K. Scalable Molecular Dynamics with NAMD. J. Comput. Chem. 2005; 26:1781–1802. [PubMed: 16222654]

31. MacKerell AD, Bashford D, Bellott M, Dunbrack RL, Evanseck JD, Field MJ, Fischer S, Gao J, Guo H, Ha S, et al. All-Atom Empirical Potential for Molecular Modeling and Dynamics Studies of Proteins. J. Phys. Chem. B. 1998; 102:3586–3616.

32. Mackerell AD, Feig M, Brooks CL. Extending the Treatment of Backbone Energetics in Protein Force Fields: Limitations of Gas-Phase Quantum Mechanics in Reproducing Protein Conformational Distributions in Molecular Dynamics Simulations. J. Comput. Chem. 2004; 25:1400–1415. [PubMed: 15185334]

33. Martyna GJ, Tobias DJ, Klein ML. Constant Pressure Molecular Dynamics Algorithms. J. Chem. Phys. 1994; 101:4177–4189.

34. Feller SE, Venable RM, Pastor RW. Computer Simulation of a DPPC Phospholipid Bilayer: Structural Changes as a Function of Molecular Surface Area. Langmuir. 1997; 13:6555–6561.

35. Ryckaert JP, Ciccotti G, Berendsen HJ. C. Numerical-Integration of Cartesian Equations of Motion of a System With Constraints-Molecular-Dynamics of N-Alkanes. J. Comput. Phys. 1977; 23:327–341.

36. Wang H-F, Gan W, Lu R, Rao Y, Wu B-H. Quantitative Spectral and Orientational Analysis in Surface Sum Frequency Generation Vibrational Spectroscopy (SFG-VS). Int. Rev. Phys. Chem. 2005; 24:191–256.

37. Nihonyanagi S, Yamaguchi S, Tahara T. Direct Evidence for Orientational Flip-Flop of Water Molecules at Charged Interfaces: A Heterodyne-Detected Vibrational Sum Frequency Generation Study. J. Chem. Phys. 2009; 130:204704. [PubMed: 19485472]

38. Gragson DE, Richmond GL. Investigations of the Structure and Hydrogen Bonding of Water Molecules at Liquid Surfaces by Vibrational Sum Frequency Spectroscopy. J. Phys. Chem. B. 1998; 102:3847–3861.

39. Yeganeh MS, Dougal SM, Pink HS. Vibrational Spectroscopy of Water at Liquid/Solid Interfaces: Crossing the Isoelectric Point of a Solid Surface. Phys. Rev. Lett. 1999; 83:1179–1182.

40. Lucarini, V.; Saarinen, JJ.; Peiponen, K-E.; Vartiainen, EM. Kramers-Kronig Relations in Optical Materials Research. Springer; New York: 2005.

41. Hirose C, Akamatsu N, Domen K. Formulas for the Analysis of the Surface SFG Spectrum and Transformation Coefficients of Cartesian SFG Tensor Components. Appl. Spectrosc. 1992; 46:1051–1072.

42. Simpson GJ, Perry JM, Ashmore-Good CL. Molecular and Surface Hyperpolarizability of Oriented Chromophores of Low Symmetry. Phys. Rev. B. 2002; 66:165437.

43. Essmann U, Perera L, Berkowitz ML, Darden T, Lee H, Pedersen LG. A Smooth Particle Mesh Ewald Method. J. Chem. Phys. 1995; 103:8577–8593.

44. Rivard M, Laliberté M, Bertrand-Grenier A, Harnagea C, Pfeffer CP, Vallieres M, St-Pierre Y, Pignolet A, El Khakani MA, Légaré F. The Structural Origin of Second Harmonic Generation in Fascia. Biomed. Opt. Express. 2011; 2:26–36. [PubMed: 21326632]

45. Harnagea C, Vallieres M, Pfeffer CP, Wu D, Olsen BR, Pignolet A, Légaré F, Gruverman A. Two-Dimensional Nanoscale Structural and Functional Imaging in Individual Collagen Type I Fibrils. Biophys. J. 2010; 98:3070–3077. [PubMed: 20550920]

46. Birk DE, Zycband EI, Winkelmann DA, Trelstad RL. Collagen Fibrillogenesis In Situ: Fibril Segments Are Intermediates in Matrix Assembly. Proc. Natl. Acad. Sci. U.S.A. 1989; 86:4549–4553. [PubMed: 2734306]
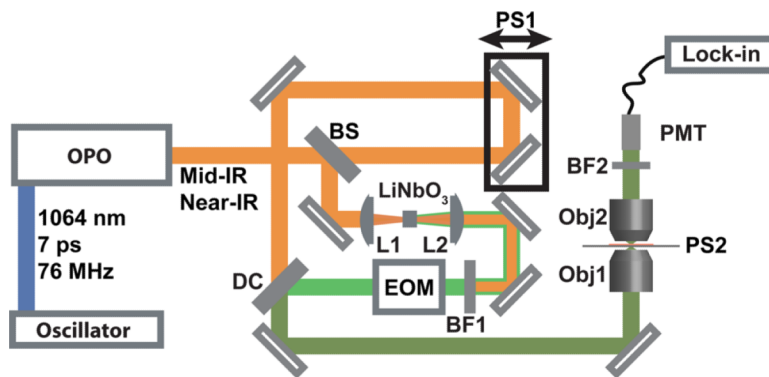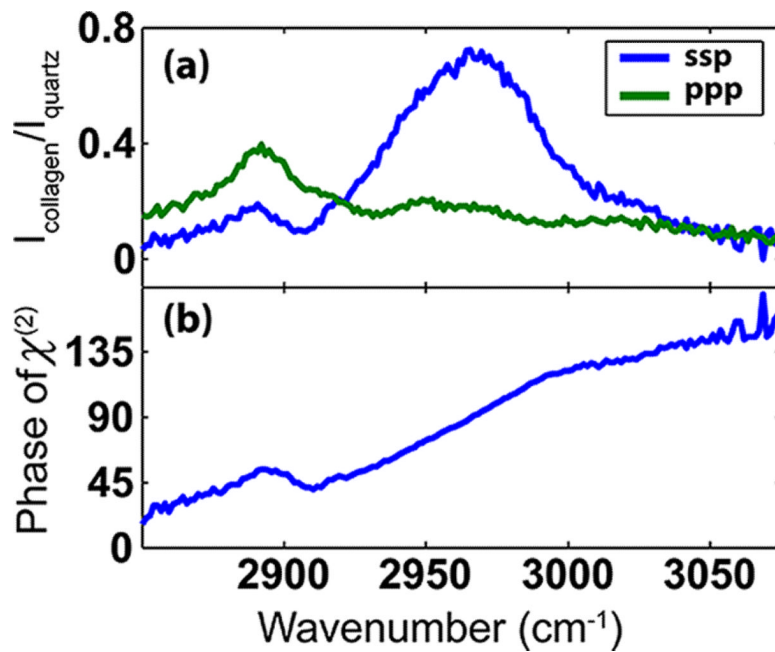
Figure 1.
The schematics of the PSVR-SFG setup. BS, 50/50 beam splitter for both near-IR and mid-IR; L1, L2, plano-convex lenses; PS1, linear delay stage with a piezo pad; PS2, 2D piezo stage; BF1, BF2, band-pass filter; EOM, electro-optic phase modulator; DC, customized dichroic that reflects the LO and passes near- and mid-IR; Obj1, 0.65 NA 74× reflective objective; Obj2, 0.75 NA 20× objective; PMT, photomultiplier tube.
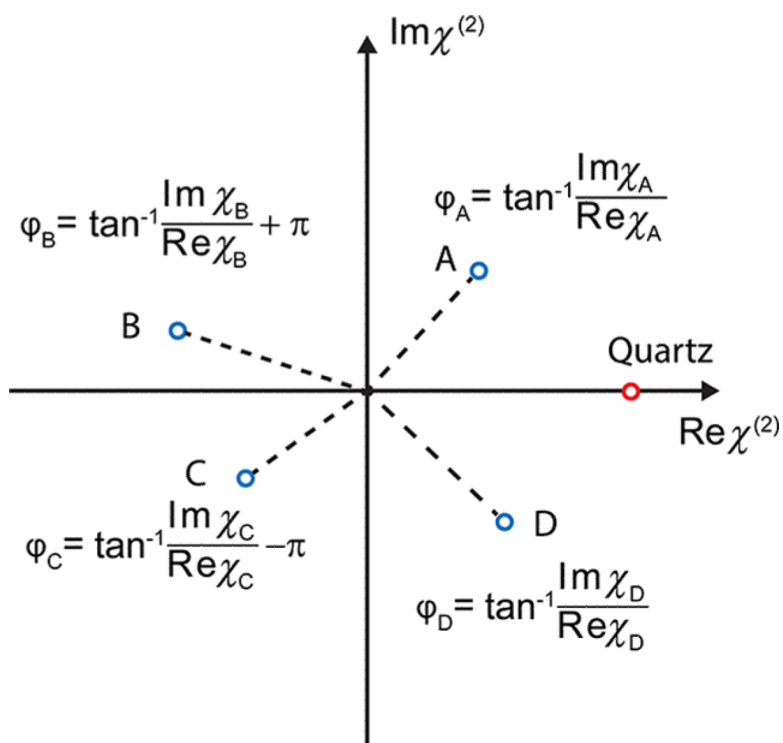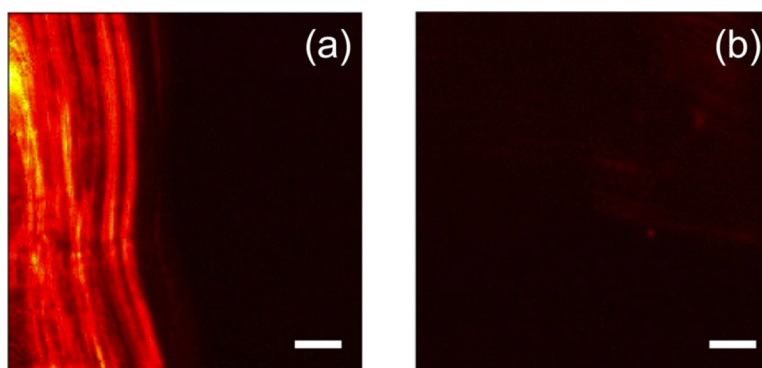
Figure 2.
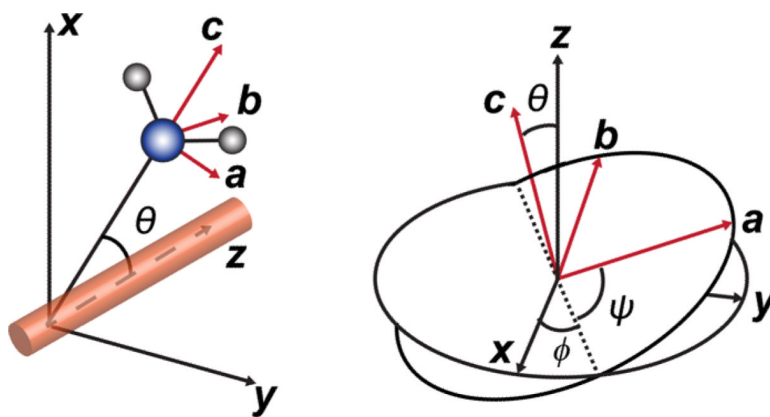The schematics of the phase definition.

Figure 3.
(a) VR-SFG spectra of collagen fibers from rat tail tendon tissue taken with different

polarizations. (b) The phase of $\chi^{(2)}_{ssp}$ calculated from the ssp polarization spectrum of collagen fibers.
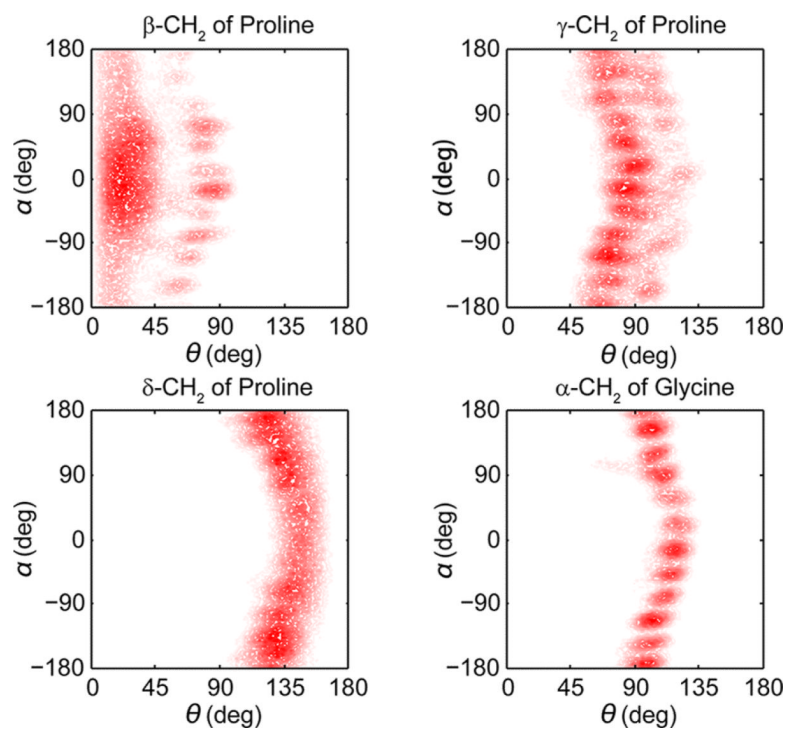
Figure 4.
Polarization dependent homodyne detected VR-SFG images of rat tail tendon tissue. The orientation of tendon tissue was placed (a) parallel and (b) perpendicular to the mid-IR polarization. The scale bar is 20 μm.
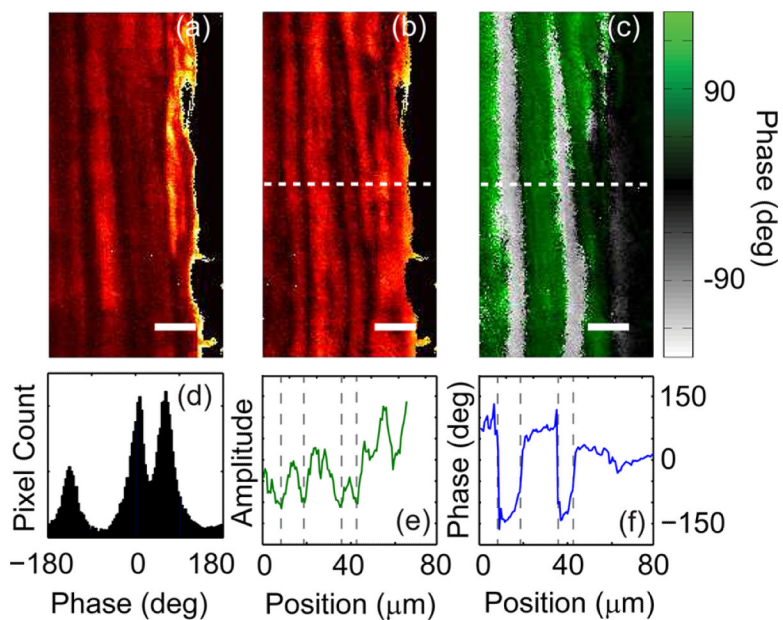
Figure 5.
VR-SFG images of rat tail tendon tissue on top of *z*-cut quartz: (a) intensity image from homodyne detection; (b) amplitude and (c) phase images from heterodyne detection. The black regions close to the right edges of images indicate the regions corresponding to quartz. (d) The phase distribution of the whole image in panel c. (e) A slice through the amplitude image along the dashed line. (f) A slice through the amplitude image along the dashed line. Note that the quartz response in panels a and b were set to zero to emphasize the details of the tendon tissue. The scale bar is 20 *μ*m.

Figure 6.
The schematic of methylene group orientation in the molecular and laboratory coordinates and the definition of Euler angles θ, φ, and ψ.

Figure 7.
Orientation distribution of the different CH_2 groups with respect to the principal axes of the $[(PPG)_{10}]_3$ triple helix. The angle θ is defined as the angle between the c-axis of the methylene group and the longitudinal axis of the triple helix. The angle α is the azimuthal angle.